Time and Frequency Response of a Resistance-Wire Aircraft Atmospheric Temperature Sensor

G. A. PAYNE, C. A. FRIEHE, AND D. K. EDWARDS

Department of Mechanical and Aerospace Engineering, University of California, Irvine, Irvine, California

(Manuscript received 13 October 1992, in final form 29 July 1993)

ABSTRACT

The heat transfer characteristics of an aircraft-mounted resistance-wire atmospheric temperature sensor are modeled to determine the time and frequency responses. The sensor element (Rosemount 102E4AL) consists of a 25-μm-diameter platinum wire wound around a cruciform mica support with approximately 143 diameters of wire between contacts with the mica. A longitudinally distributed, radially lumped capacitance model provided for the convective heat transfer to the wire and the transient heat conduction along it. Similarly, the temperature gradient across the thin dimension of the mica support was neglected, and a radially distributed model provided for the convective heat transfer to the mica and the transient conduction within it. The two solutions are coupled by the boundary conditions at the wire–mica contact. The equations were solved to produce the temperature distribution along the wire and in the mica support as a function of the frequency of a free-stream sinusoidal temperature fluctuation. The frequency response transfer function was determined and fit to a two-time-constant transfer function by regression analysis. The two-time-constant model fits the general solution very well. The small (fast response) time constant is essentially determined by the wire itself. The larger (slow response) time constant is due to conduction into and out of the mica supports. The model predicts that the effects of the mica supports are important for frequencies greater than about 0.1 Hz. The responses to five different temperature waveform inputs (sinusoid, step, pulse, ramp, and ramp level) are derived using the two-time-constant model with Laplace transform techniques for both infinite-length wire (no mica support effects) and the finite-length wire of the 102 probe. The actual temperature signals are distorted by the larger time constant of the mica supports, especially for the pulse and ramp inputs that are typical of aircraft measurements of thermals and inversions.

1. Introduction

Resistance-wire temperature sensors in aerodynamic housings are used to measure total air temperature for the calculation of true airspeed and to sense turbulent air temperature by research aircraft. The Rosemount model 102 probe[1] (hereafter called the 102 probe) is commonly used but has been noted to have a two-time-constant response (Rosemount 1963; Lenschow 1972; Friehe and Khelif 1993). The 102 probe consists of a housing that inertially separates out water droplets and an internal platinum wire sensor that is wound around a structure of four thin mica supports. It has been proposed that conduction to the supports is a reason for at least part of the two-time-constant response. In the present work the transient heat conduction in the wire and support is analyzed to determine the time and frequency responses.

The 102 probe is shown in Fig. 1, and the internal sensor consisting of the 25-μm-diameter platinum wire wound on the cruciform mica supports is shown in the photograph in Fig. 2. The wire length between two mica supports is about 3630 μm, giving a length-to-diameter (l/d) ratio of 143. Paranthoen et al. (1982) have shown that small l/d ratios adversely affect the time–frequency response of temperature wires due to heat conduction to metal wire supports as used in laboratory probes. Observations of the time response of the 102 probe from in-flight data by several investigators (e.g., Lenschow 1972; Friehe and Khelif 1993) have shown two time constants, but the values of the larger time constant differ.

In the present work, the finite-length wire and its mica support assembly are analyzed as transient heat transfer "fin" problems, with the solutions coupled by the boundary conditions at the wire-support interface. The resulting differential equations are solved, and it is shown that the spatially averaged wire temperature can be closely represented by a two-time-constant model. The time constants found are compared to previous results and the analytical solution for the limiting case of an infinite-length wire. The frequency response transfer function is derived, and amplitude and phase-shift predictions for the 102 probe are calculated and compared to the infinite-length wire case.

[1] Model 102E4AL of Rosemount Engineering, Eagan, Minnesota.

Corresponding author address: Dr. Carl A. Friehe, Department of Mechanical Engineering, University of California, Irvine, CA 92717.

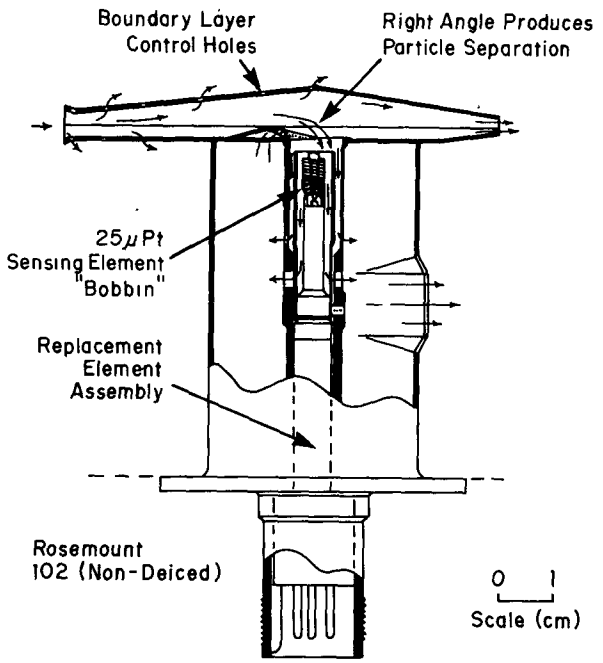

FIG. 1. Schematic of the Rosemount 102 nondeiced temperature probe and housing (permission to copy figure courtesy of Rosemount Engineering Company).

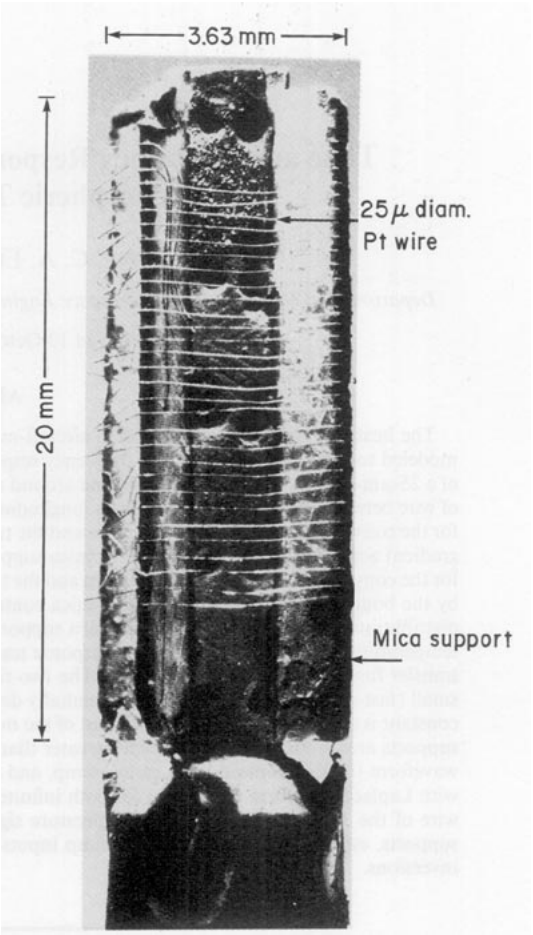

FIG. 2. Photograph of the 102 probe sensing element.

2. Theory

a. *Finite-length wire*

1) MODEL DEVELOPMENT

The uniform winding of the wire on the supports allows the probe to be modeled as a repetitive array of cells, each cell consisting of a half-span of wire attached to half of a mica support (Figs. 3 and 4). The properties of the wire, mica, and atmospheric conditions used are given in Table 1. The velocity of the airstream is assumed to be 10 m s^{-1} for the restricted flow in the 102 housing. [In a wind tunnel test with the free-stream speed of 72 m s^{-1}, the speed inside the 102 housing was given as 8.4 m s^{-1} by R. Schwiesow (1993, personal communication).] In general, the speed of the airstream flowing over the probe is a function of the aircraft airspeed. The wire properties and the thinness of the mica allow each to be modeled as a lumped capacitance in the thin direction but not in the long direction, since the respective Biot numbers, based on the thin dimensions, are less than 0.1 (Incropera and DeWitt 1985). Namely, we can neglect radial temperature gradients in the wire, and across-support temperature gradients in the mica.

A heat balance is made on a differential length dz of the wire including conduction along the wire, loss by convection to the airstream, and resistive heating due to the sensing current and neglecting radiation due to the low wire emissivity. The result is

$$\rho_w c_w A_c \frac{\partial T_w}{\partial t} = k_w A_c \frac{\partial^2 T_w}{\partial z^2} + \frac{I^2 \rho_e}{A_c} - 2\pi r_w h_w (T_w - T_e), \quad (1)$$

where T_w is the wire temperature, T_e the environmental temperature, $A_c = \pi r_w^2$, r_w is the wire radius, z the axial coordinate, h_w the wire convective heat transfer coef-

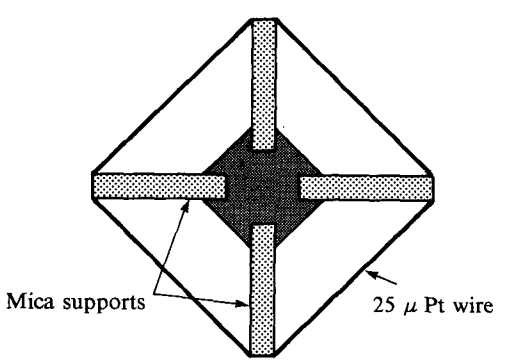

FIG. 3. Schematic of top view of 102 probe sensing element.

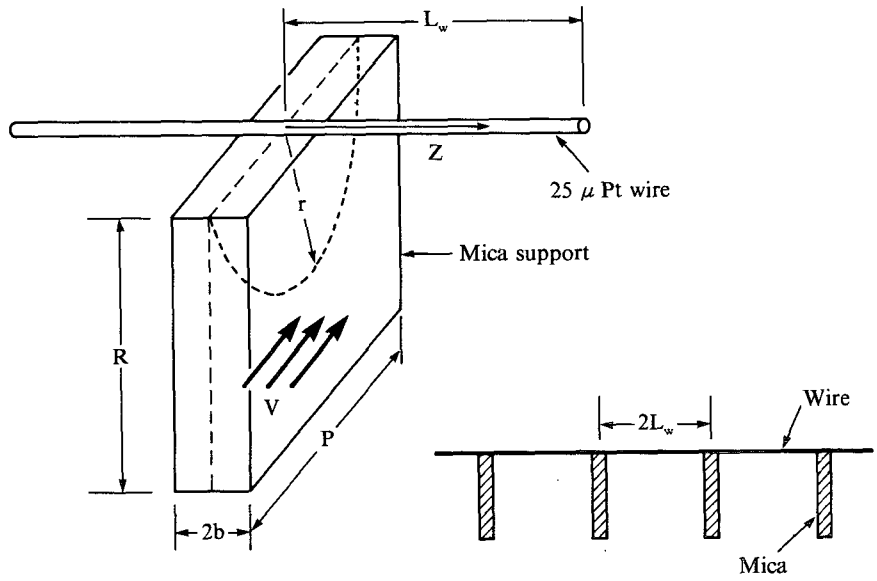

FIG. 4. Schematic of platinum wire and mica support. Airspeed vector **V** shown normal to wire.

ficient, I the wire current (constant), ρ_e the wire electrical resistivity, k_w the wire thermal conductivity, c_w the wire specific heat, ρ_w the wire density, and t the time.

A heat balance for the mica for a half-annulus between radii r and $r + dr$ (Fig. 5) includes heat flow in by conduction from the positive r direction and heat flow out by conduction at $r + dr$ and by convection at the mica surface. The midplane of the mica is an adiabatic surface due to symmetry. The governing differential equation for the mica is

$$rb\rho_m c_m \frac{\partial T_m}{\partial t} = \frac{\partial}{\partial r}\left(rbk_m \frac{\partial T_m}{\partial r}\right) - rh_m(T_m - T_e), \quad (2)$$

where T_m is the mica temperature, h_m the mica convective heat transfer coefficient, ρ_m the mica density, c_m the mica specific heat, k_m the mica thermal conductivity, b the mica half-thickness, and r the radial coordinate.

TABLE 1. Wire, mica, and atmospheric conditions.

Wire geometry		
r_w	12.7 μm	wire radius
L_w	1.82 mm	mica-to-midspan wire length
Wire parameters		
I	1 mA	sensing current
ρ_e	98.3 $\mu\Omega$ m	resistivity
k_w	73 W m^{-1} K^{-1}	thermal conductivity
ρ_w	2.145×10^4 kg m^{-3}	density
c_w	134 J kg^{-1} K^{-1}	specific heat
Mica geometry		
b	88.9 μm	mica half-thickness
P	127 μm	pitch between the wires
R	1.473 mm	height, from tip to base
Mica parameters		
k_m	0.588 W m^{-1} K^{-1}	thermal conductivity
ρ_m	2.845×10^3 kg m^{-3}	density
c_m	863 J kg^{-1} K^{-1}	specific heat
Atmospheric parameters		
T_0	300 K	ambient temperature
P_0	101.3 kPa	ambient pressure
V	10 m s^{-1}	velocity
ν	15.7×10^{-6} m^2 s^{-1}	kinematic viscosity
k_a	0.0267 W m^{-1} K^{-1}	thermal conductivity
Pr	0.69	Prandtl number

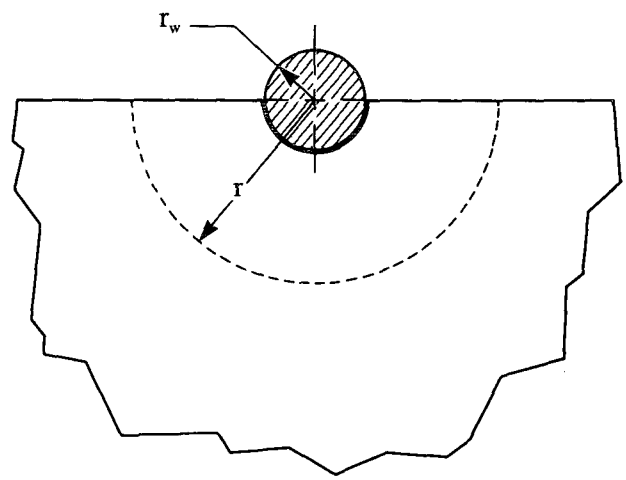

FIG. 5. Wire-end view of Fig. 4 showing wire–mica contact at $r = r_w$.

The convective heat transfer coefficient for the wire, h_w, is that for forced convection and is parameterized as the Nusselt number, $\mathrm{Nu}_w = 2r_w h_w / k_a$. For Reynolds numbers (based on wire diameter and velocity V) in the range 0.02–44, Collis and Williams (1956) found for air

$$\mathrm{Nu}_w \equiv \frac{2r_w h_w}{k_a} = A + B\,\mathrm{Re}_w^n, \tag{3}$$

where

$$\mathrm{Re}_w \equiv \frac{2r_w V}{\nu}, \tag{4}$$

and A, B, and n were 0.24, 0.56, and 0.45, respectively.

For extremely fine diameter wires or low pressures, rarefied gas effects must be taken into account, as given in the Appendix.

The heat transfer coefficient for the mica fin, h_m, is obtained in a like manner with $\mathrm{Nu}_m = h_m L_m / k_a$, where L_m is the characteristic length of mica exposed to the flow. For the first turn of wire, Nu_m is taken to be the flat-plate Nusselt number averaged over L_m, equal to one wire pitch P:

$$\mathrm{Nu}_m = 2\,\mathrm{Nu}_x = 2 \times 0.332\,\mathrm{Re}_{x=P}^{1/2}(\mathrm{Pr})^{1/3}.$$

The Reynolds number is

$$\mathrm{Re}_x = \frac{Vx}{\nu},$$

where x is the local position from the windward edge of the mica and Pr is the Prandtl number (e.g., Edwards et al. 1979, p. 166).

With the introduction of the definitions

$$\alpha_w \equiv \frac{k_w}{\rho_w c_w}, \quad \alpha_m \equiv \frac{k_m}{\rho_m c_m}$$

$$\lambda_w^2 \equiv \frac{2h_w}{r_w k_w}, \quad \lambda_m^2 \equiv \frac{h_m}{b k_m}$$

$$\tilde{\omega}_w \equiv \lambda_w^2 \alpha_w, \quad \tilde{\omega}_m \equiv \lambda_m^2 \alpha_m, \quad \text{and}$$

$$T_c \equiv \frac{I^2 \rho_e r_w}{2h_w A_c^2},$$

Eqs. (1) and (2) become

$$\frac{\partial T_w}{\partial t} = \alpha_w \frac{\partial^2 T_w}{\partial z^2} - \tilde{\omega}_w T_w + \tilde{\omega}_w T_c + \tilde{\omega}_w T_e, \tag{5}$$

$$r^2 \frac{\partial T_m}{\partial t} = r\alpha_m \frac{\partial T_m}{\partial r} + r^2 \alpha_m \frac{\partial^2 T_m}{\partial r^2} - \tilde{\omega}_m T_m + \tilde{\omega}_m T_e. \tag{6}$$

(The quantity $\tilde{\omega}_w$ will be seen later to be the −3-dB frequency value for the wire.) The boundary and initial conditions on the wire are

- at $z = L_w$, adiabatic due to symmetry at the midspan,
- at $z = 0$, temperature and heat flow are continuous across the wire–mica interface,
- at $t = 0$, the wire is hotter, $T_0 + T_c$, than the environmental temperature T_0 due to I^2R heating,

and for the mica

- mica temperature remains finite at large r,
- at $r = r_w$, temperature and heat flow are continuous across the wire–mica interface, and
- at $t = 0$, the mica is at the environmental temperature T_0.

For one solution of the above set of equations, the temperature of the airstream T_e is assumed to have a sinusoidal fluctuation of magnitude ΔT_0 and frequency ω:

$$T_e(\omega, t) = T_0 + e^{i\omega t}\Delta T_0. \tag{7}$$

For this steady periodic condition, the wire and mica respond sinusoidally in time with spatially dependent phase lag and attenuation; that is,

$$T_w(\omega, z, t) = T_{w0}(z) + e^{i\omega t}F_w(\omega, z), \tag{8}$$

$$T_m(\omega, r, t) = T_{m0}(r) + e^{i\omega t}F_m(\omega, r), \tag{9}$$

where T_{w0}, T_{m0}, F_w, and F_m are the response functions to be determined. Substituting Eqs. (7) and (8) into Eq. (5) produces two ordinary differential equations, one in $T_{w0}(z)$, real, and the other in $F_w(\omega, z)$, complex:

$$\frac{d^2 T_{w0}}{dz^2} - \lambda_w^2 T_{w0} = -\lambda_w^2 T_{w,t}, \tag{10}$$

$$\frac{d^2 F_w}{dz^2} - \Gamma_w^2 F_w = -\lambda_w^2 \Delta T_0, \tag{11}$$

where $\Gamma_w^2 \equiv \lambda_w^2 + iw\alpha_w^{-1}$ and $T_{w,t} \equiv T_0 + T_c$. A similar approach is used for the mica giving

$$r^2 \frac{d^2 T_{m0}}{dr^2} + r \frac{dT_{m0}}{dr} - r^2 \lambda_m^2 T_{m0} = -\lambda_m^2 T_0, \tag{12}$$

$$r^2 \frac{d^2 F_m}{dr^2} - r \frac{dF_m}{dr} - r^2 \Gamma_m^2 F_m = -\lambda_m^2 \Delta T_0, \tag{13}$$

where $\Gamma_m^2 \equiv \lambda_m^2 + iw\alpha_m^{-1}$. The boundary conditions now become

$$T'_{w0}(z = L_w) = 0, \quad F'_w(z - L_w) = 0, \tag{14}$$

$$T_{w0}(z = 0) = T_{m0}(r = r_w),$$

$$F_w(z = 0) = F_m(r = r_w), \tag{15}$$

$$T'_{w0}(z = 0) = -\beta T'_{m0}(r = r_w),$$

$$F'_w(z = 0) = -\beta F'_m(r = r_w), \tag{16}$$

where $\beta \equiv \lambda_w^2(2\lambda_m^2 h^*)^{-1}$, $h^* \equiv h_w / h_m$, and the prime indicates the first derivative with respect to z. The wire

and the mica are coupled only by the boundary conditions, and thus Eqs. (10)–(13) may be solved individually. The solution for the wire temperature is

$$T_{w0}(z) = T_{w,i} + [T_{w0}(0) - T_{w,i}] \times [\cosh(\lambda_w z) - \tanh(\lambda_w L_w)\sinh(\lambda_w z)], \quad (17)$$

$$F_w(\omega, z) = \frac{\lambda_w^2 \Delta T_0}{\Gamma_w^2} + \left[F_w(\omega, 0) - \frac{\lambda_w^2 \Delta T_0}{\Gamma_w^2}\right] \times [\cosh(\Gamma_w z) - \tanh(\Gamma_w L_w)\sinh(\Gamma_w z)], \quad (18)$$

and for the mica

$$T_{m0}(r) = T_0 + [T_{w0}(0) - T_0]\frac{K_0(\lambda_m r)}{K_0(\lambda_m r_w)}, \quad (19)$$

$$F_m(\omega, r) = \frac{\lambda_m^2 \Delta T_0}{\Gamma_m^2} + \left[F_w(\omega, 0) - \frac{\lambda_m^2 \Delta T_0}{\Gamma_m^2}\right]\frac{K_0(\Gamma_m r)}{K_0(\Gamma_m r_w)}, \quad (20)$$

where K_0 is the modified Bessel function of the second kind and zeroth order.

From the above equations, it is seen that the two sets of solutions are coupled by the two terms $T_{w0}(0)$ and $F_w(\omega, 0)$. Both terms are independent of space and time, but $F_w(\omega, 0)$ is a function of the input frequency ω. The effect of the mica support on the wire is through these two quantities. They account for heat flow from the wire to the mica affecting the temperature distribution in the wire and thus its electrical resistance.

The solutions for $T_{w0}(0)$ and $F_w(\omega, 0)$ are obtained from the continuous heat flow boundary condition across the wire–mica interface, Eq. (16). There results

$$T_{w0}(0) = \frac{\lambda_w T_0[K_1(\lambda_m r_w)/K_0(\lambda_m r_w)] + 2h^* T_{w,i}\lambda_m \tanh(\lambda_w L_w)}{2h^*\lambda_m \tanh(\lambda_w L_w) + \lambda_w[K_1(\lambda_m r_w)/K_0(\lambda_m r_w)]}, \quad (21)$$

$$F_w(\omega, 0) = \lambda_w^2 \Delta T_0 \times \left\{\frac{(2h^*/\Gamma_w)\tanh(\Gamma_w L_w) + (1/\Gamma_m)[K_1(\Gamma_m r_w)/K_0(\Gamma_m r_w)]}{2h^*\Gamma_w \tanh(\Gamma_w L_w) + (\lambda_w^2/\lambda_m^2) \times \Gamma_m[K_1(\Gamma_m r_w)/K_0(\Gamma_m r_w)]}\right\}, \quad (22)$$

where K_1 is the modified Bessel function of the second kind and first order.

With the dependence of the wire temperature at the mica interface given by Eqs. (21) and (22), the response of the wire to T_e, the fluctuating environmental temperature, can be determined.

2) TRANSFER FUNCTION

The actual measured temperature of a wire is obtained from the integrated electrical resistance over its length, which is controlled by the average temperature over the length. Therefore, Eq. (8) is averaged over the half-span L_w:

$$\bar{T}_w(\omega, t) = \frac{1}{L_w}\int_0^{L_w} T_w(\omega, z, t)dz, \quad (23)$$

$$\bar{T}_{w0} = T_{w,i} + [T_{w0}(0) - T_{w,i}]\frac{\tanh(\lambda_w L_w)}{\lambda_w L_w}, \quad (24)$$

$$\bar{F}_w(\omega) = \frac{\lambda_w^2 \Delta T_0}{\Gamma_w^2} + \left[F_w(\omega, 0) - \frac{\lambda_w^2 \Delta T_0}{\Gamma_w^2}\right]\frac{\tanh(\Gamma_w L_w)}{\Gamma_w L_w}, \quad (25)$$

where the overbar indicates the spatial average. Equation (25) is thus the response of the wire about the mean temperature given by Eq. (24). From control theory the system transfer function is defined as the ratio of the output to the input:

$$H_w(\omega) = \frac{\bar{F}_w}{\Delta T_0} = \frac{\lambda_w^2}{\Gamma_w^2} + \left[\frac{F_w(\omega, 0)}{\Delta T_0} - \frac{\lambda_w^2}{\Gamma_w^2}\right]\frac{\tanh(\Gamma_w L_w)}{\Gamma_w L_w}. \quad (26)$$

The transfer function is complex [in Γ_w^2 and $F_w(\omega, 0)$] and is expressed equivalently as the amplitude ratio $M_w(\omega)$, and phase shift $\Phi_w(\omega)$:

$$M_w(\omega) = |H_w|, \quad (27)$$

$$\Phi_w(\omega) = \angle H_w. \quad (28)$$

b. Infinite-length wire

1) MODEL DEVELOPMENT

The limiting case of an infinite-length wire for which the effect of the mica becomes negligible is readily extracted. For this case, the z dependence in Eq. (1) is zero and

$$\rho_w c_w A_c \frac{\partial T_{w,\infty}}{\partial t} = \frac{I^2 \rho_e}{A_c} - 2\pi r_w h_w (T_{w,\infty} - T_e), \quad (29)$$

with the initial condition $T_{w,\infty}(t = 0) = T_{w,i}$. The solution is again of the form

$$T_{w,\infty}(\omega, t) = T_{w0,\infty} + e^{i\omega t} F_{w,\infty}(\omega), \quad (30)$$

with the input T_e given by Eq. (7). As before, Eqs. (7) and (30) are substituted into Eq. (29), which gives two constants, as compared to the finite-length case, that resulted in two differential equations:

$$T_{w0,\infty} = T_{w,i},$$

$$F_{w,\infty}(\omega) = \frac{\lambda_w^2 \Delta T_0}{\Gamma_w^2},$$

or

$$T_{w,\infty}(\omega, t) = T_{w,i} + \frac{\lambda_w^2 \Delta T_0}{\Gamma_w^2} e^{i\omega t}. \tag{31}$$

2) TRANSFER FUNCTION

The infinite-length wire transfer function is given by

$$H_{w,\infty}(\omega) = \frac{F_{w,\infty}}{\Delta T_0} = \frac{\lambda_w^2}{\Gamma_w^2} = \frac{\tilde{\omega}_w}{\tilde{\omega}_w + i\omega}, \tag{32}$$

and, as before,

$$M_{w,\infty}(\omega) = |H_{w,\infty}|, \tag{33}$$

$$\Phi_{w,\infty}(\omega) = \angle H_{w,\infty}. \tag{34}$$

A comparison is obtained when $L_w \to \infty$ in Eqs. (24) and (25) for the averaged finite-length wire:

$$\lim_{L_w \to \infty} \bar{T}_{w0} = T_{w,i},$$

$$\lim_{L_w \to \infty} \bar{F}_w(\omega) = \frac{\lambda_w^2 \Delta T_0}{\Gamma_w^2}.$$

Thus,

$$\lim_{L_w \to \infty} \bar{T}_w(\omega, t) = T_{w,i} + \frac{\lambda_w^2 \Delta T_0}{\Gamma_w^2} e^{i\omega t}, \tag{35}$$

which is the same as Eq. (31).

The transfer function $H_{w,\infty}$ can also be expressed as a function of $s = i\omega$ so that Laplace transform methods can be used to determine different outputs for a given input:

$$H_{w,\infty}(s) = \frac{\tilde{\omega}_w}{\tilde{\omega}_w + s}. \tag{36}$$

c. Two-time-constant transfer function

Rosemount (1963) suggests the following equation with two time constants to describe the response of the 102 probe to a temperature step change:

$$\frac{T_f - T_{w,tt}}{T_f - T_{w,i}} = a_1 e^{-\omega_1 t} + a_2 e^{-\omega_2 t} \tag{37}$$

with

$$a_1 + a_2 = 1,$$

where $T_{w,tt}$ is the two-time-constant model (TTCM) wire temperature, ω_1 and ω_2 are the two reciprocal time constants, and T_f is the final temperature reached by the probe, $T_{w,i} + \Delta T_0$. The influences of the mica and wire properties are contained in the empirical time constants ω_1^{-1} and ω_2^{-1} and a_1 (or a_2). Rosemount attributes ω_1 to the platinum wire ("sensing element") and ω_2 to the probe housing (i.e., mica supports, probe support post, and gold-plated inner radiation shield and housing).

It is of interest to compare the response given by the empirical formula of Eq. (37) to that of the present model for the finite-length wire case.

The Laplace transform of $T_{w,tt} - T_{w,i}$ is

$$\mathcal{L}[T_{w,tt}(t) - T_{w,i}] = \mathcal{L}[\Delta T_0(1 - a_1 e^{-\omega_1 t} - a_2 e^{-\omega_2 t})],$$

$$= \Delta T_0 \left(\frac{1}{s} - \frac{a_1}{s + \omega_1} - \frac{a_2}{s + \omega_2} \right). \tag{38}$$

Since Eq. (38) is the response to a step input $\Delta T_0 s^{-1}$, the transfer function is then

$$H_{w,tt}(s) = 1 - \frac{a_1 s}{s + \omega_1} - \frac{a_2 s}{s + \omega_2}. \tag{39}$$

Equation (26) can be written as

$$H_w(s) = \frac{\tilde{\omega}_w}{s + \tilde{\omega}_w} + \frac{\alpha_w^{1/2}}{L_w} \left[\frac{F_w(\omega, 0)}{\Delta T_0} - \frac{\tilde{\omega}_w}{s + \tilde{\omega}_w} \right] \frac{\tan\{[(s + \tilde{\omega}_w)/\alpha_w]^{1/2} L_w\}}{(s + \tilde{\omega}_w)^{1/2}} \tag{40}$$

for comparison to Eq. (39). Since the inverse transform of Eq. (40) is complicated, we chose to use a regression analysis to compare the time response of the Rosemount two-time-constant model to our model.

The undetermined parameters in Eq. (37) are the two reciprocal time constants, ω_1 and ω_2 and either a_1 or a_2 (since $a_1 + a_2 = 1$). To compare the two-time-constant model to the finite-length wire model, $i\omega$ is substituted for s in Eq. (39) so that the amplitude ratio and phase shift can be obtained:

$$H_{w,tt}(\omega) = 1 - \frac{a_1 i\omega}{i\omega + \omega_1} - \frac{a_2 i\omega}{i\omega + \omega_2}, \tag{41}$$

$$M_{w,tt}(\omega) = \left[\frac{(a_1\omega_1 + a_2\omega_2)^2 \omega^2 + (\omega_1\omega_2)^2}{(\omega_1^2 + \omega^2)(\omega_2^2 + \omega^2)} \right]^{1/2}, \tag{42}$$

$$\Phi_{w,tt}(\omega) = -\tan^{-1}\left[\omega \frac{a_1\omega_1(\omega_2^2 + \omega^2) + a_2\omega_2(\omega_1^2 + \omega^2)}{\omega^2(a_1\omega_1^2 + a_2\omega_2^2) + (\omega_1\omega_2)^2} \right]. \tag{43}$$

Equation (42) is then compared to Eq. (27) so that the unknown parameters can be determined.

A Gauss–Newton nonlinear regression was used to solve for ω_1, ω_2, and a_2 in Eq. (42) (Chapra and Canale 1988, p. 358). To simplify the regression, only first-order terms of a Taylor series expansion in each un-

known were used. The difference in the models (i.e., the residual) is

$$M_w^l(\omega_j) - M_{w,tl}^l(\omega_j) = \frac{\partial M_{w,tl}(\omega_j)}{\partial a_2}\Delta a_2 + \frac{\partial M_{w,tl}(\omega_j)}{\partial \omega_1}\Delta\omega_1 + \frac{\partial M_{w,tl}(\omega_j)}{\partial \omega_2}\Delta\omega_2, \quad (44)$$

where l is the iteration number, $j: 1 \rightarrow N$, and N is the number of points used in Eqs. (27) and (42). A least-squares method was employed to evaluate ω_1, ω_2, and a_2. Equation (44) is written as a matrix equation:

$$(\mathbf{Z}_l^T\mathbf{Z}_l)\Delta\mathbf{A}_l = \mathbf{Z}_l^T\mathbf{D}$$

or

$$\mathbf{A}_{l+1} = \mathbf{A}_l + (\mathbf{Z}_l^T\mathbf{Z}_l)^{-1}\mathbf{Z}_l^T\mathbf{D}, \quad (45)$$

where

$$\mathbf{Z}_l = \left[\frac{\partial M_{w,tl}(\omega_j)}{\partial a_2}\ \frac{\partial M_{w,tl}(\omega_j)}{\partial \omega_1}\ \frac{\partial M_{w,tl}(\omega_j)}{\partial \omega_2}\right]$$

$$\mathbf{A}_{l+1} = \begin{bmatrix} a_{2,l+1} \\ \omega_{1,l+1} \\ \omega_{2,l+1} \end{bmatrix}; \quad \mathbf{A}_l = \begin{bmatrix} a_{2,l} \\ \omega_{1,l} \\ \omega_{2,l} \end{bmatrix}$$

and

$$\mathbf{D} = [\mathbf{M}_w^l(\omega_j) - \mathbf{M}_{w,tl}^l(\omega_j)].$$

The iteration procedure was the following.

1) Choose initial values of ω_1, ω_2, and a_2.
2) Determine $M_{w,tl}$ for all ω_j points and subtract it from the finite-length wire model [Eq. (27)], evaluated at all the same ω_j points to form matrix $\mathbf{D}$.
3) Determine the rms of the difference between the models,

$$\text{rms} = \frac{\text{norm}(\mathbf{D})}{N^{1/2}},$$

and stop the iteration when it reached 0.0027.

3. Results

a. Transfer function

The complete solution for the finite-length wire allows the transfer function for the wire to be determined as a function of distance along the wire and frequency:

$$M_{w,z}(\omega) = \left|\frac{F_w(\omega, z)}{\Delta T_0}\right|$$

$$\Phi_{w,z}(\omega) = \angle\left[\frac{F_w(\omega, z)}{\Delta T_0}\right].$$

These are plotted in perspective in Fig. 6 and show the influence of the mica support in the region around $z = 0$. The attenuation at high frequencies is clearly evident at the end of the wire near the mica. Similar observations apply to the phase shift. At the midpoint of the wire, $z = L_w$, the wire response approaches the behavior of an infinite-length wire [Eq. (33)], which is due to L_w being large compared to a characteristic heat transfer fin length L_e:

$$L_e = \left(\frac{k_w A_c}{h_w \mathcal{P}}\right)^{1/2} = \left(\frac{r_w k_w}{2h_w}\right)^{1/2} = \frac{1}{\lambda_w},$$

where $\mathcal{P}$ is the perimeter of the wire. Here the wire is thought of as a cylindrical heat transfer fin. The length L_e is the length along an infinite-length heat transfer fin at which the temperature difference falls by e^{-1}. A fin three or four times this length is essentially an infinite-length fin (Edwards et al. 1979, 32–33). For the

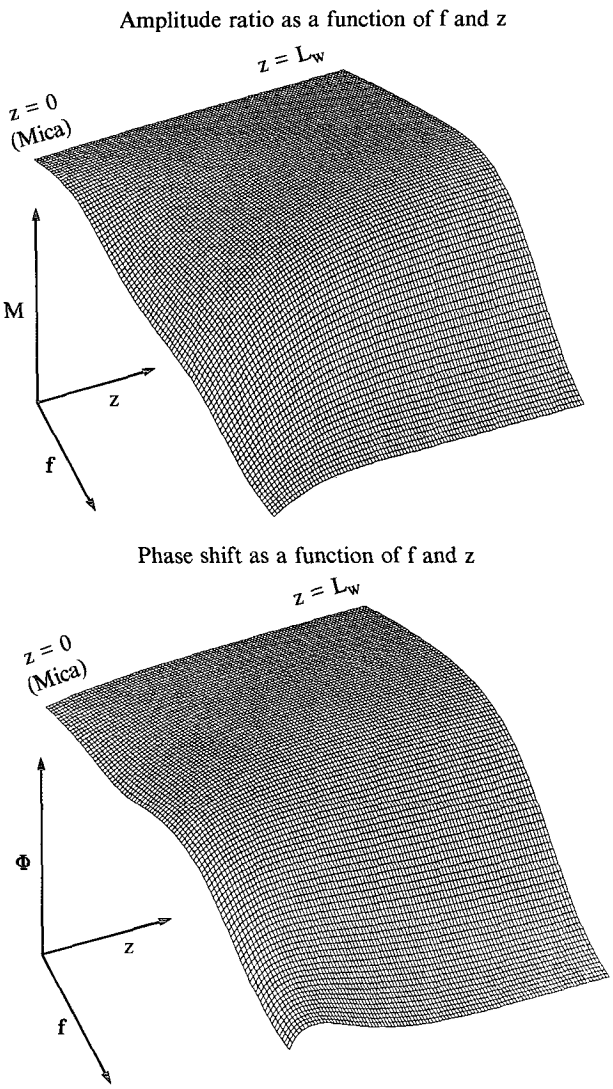

FIG. 6. Perspective view of transfer function amplitude $M_{w,z}(f)$ and phase $\Phi_{w,z}(f)$ as a function of distance z along the wire and frequency f.

102 probe wire, $L_w/L_e \doteq 4$. Thus a significant portion of the wire near the center behaves as an infinite-length wire. Figure 7 shows the amplitude and phase shift at various distances along the wire for the 102 probe and also for an infinitely long wire.

The axially averaged finite-length wire amplitude ratio and phase-shift results [Eqs. (27) and (28)] are plotted in Fig. 8. The influence of the mica support is clearly seen as causing additional attenuation and phase shift compared to the infinitely long wire.

The transfer function of the two-time-constant model [Eq. (42)] and that of the finite-length wire model are shown in Fig. 9. The values of ω_1, ω_2, and a_2 are given in Table 2. [Wyngaard et al. (1978) reported a value of ω_1^{-1} of 0.03 for the Rosemount probe based on in-flight data; they did not report a value of ω_2^{-1}.] The difference in amplitude and phase is negligible for all practical purposes. Therefore, we can use the simplified model (with the values of ω_1, ω_2, and a_2 obtained by the regression analysis) for evaluation of the transient response.

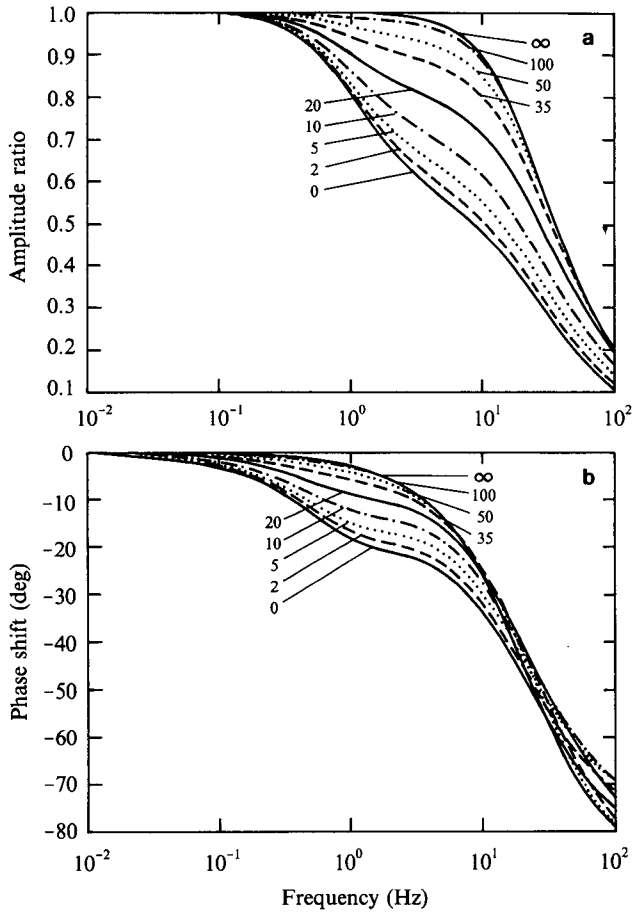

FIG. 7. Projections of Fig. 6. (a) Amplitude ratio–frequency plot and (b) phase shift–frequency plot for $z = 0$ (at mica support), 2%, 5%, 10%, 20%, 35%, 50%, and 100% of L_w (wire length). Also shown is the case for an infinitely long wire.

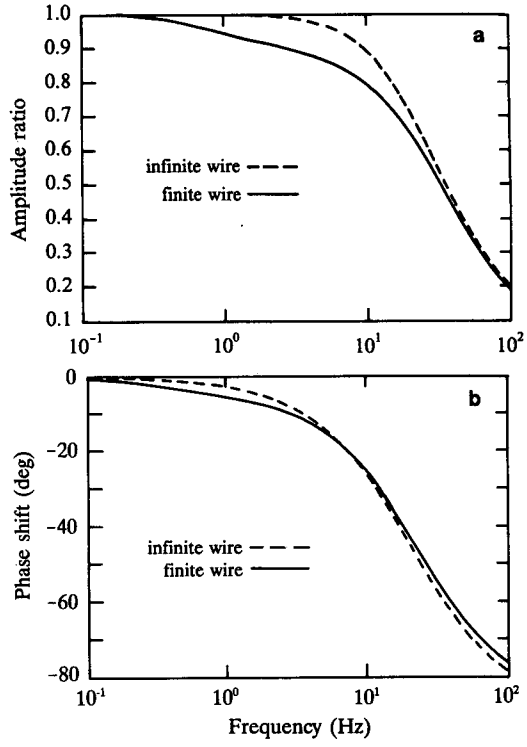

FIG. 8. Amplitude (a) and phase (b) plots of axially averaged finite-length 102 probe wire versus frequency. Also shown are the results for an infinitely long wire.

b. *Transient response*

1) INFINITE-LENGTH WIRE

The transient responses with the infinite-length wire transfer function given by Eq. (36) to five types of inputs (sinusoid, step, pulse, ramp, and angled step) are developed here to simulate various types of atmospheric temperature signals measured from research aircraft. The method employed is to multiply the Laplace transform of the input by Eq. (36) and take the inverse transform. The equation obtained is the difference between the wire temperature $T_{w,\infty}$ and its initial temperature, $T_{w,i}$.

(i) Sinusoidal input. The transform of the input is $\Delta T_0 \omega (s^2 + \omega^2)^{-1}$, where ΔT_0 is half the peak-to-peak amplitude and ω is the input frequency. The response is

$$T_{w,\infty}(\omega, t) = T_{w,i} + \Delta T_0 M_{\sim,\infty}[\sin(\omega t - \phi) + \sin(\phi)e^{-\tilde{\omega}_w t}], \quad (46)$$

where $\phi = \tan^{-1}(\omega \tilde{\omega}_w^{-1})$ and $M_{\sim,\infty} = \cos(\phi)$, the infinite-length wire phase shift and amplitude ratio, respectively. The time response to a 5-Hz sine wave is shown in Fig. 10. The response shows the attenuation and phase lag due to this relatively high-frequency forcing of the 25-μm-diameter wire and also shows the

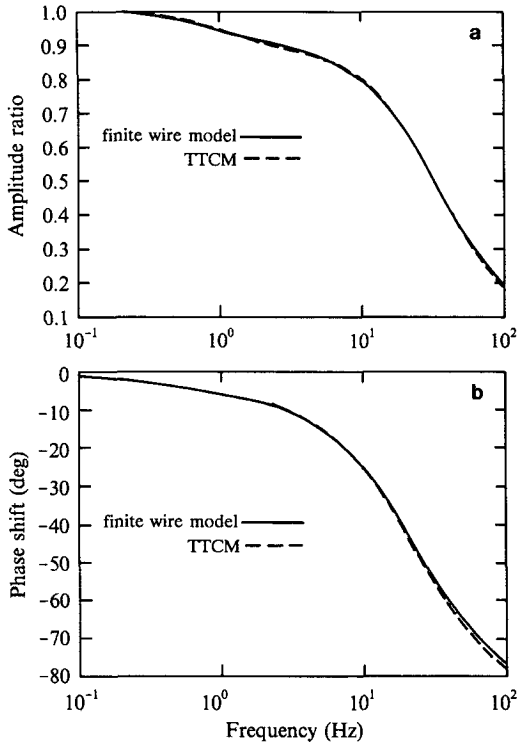

FIG. 9. Comparison of amplitude (a) and phase (b) of the finite-length wire model with the two-time-constant model obtained by regression analysis.

effect of the peak temperature reaching steady state after the first cycle after the sinusoid is switched on.

(ii) Step input. The step input simulates flight through an inversion layer. The transformed input is $\Delta T_0 s^{-1}$ where ΔT_0 is the step height. The response is

$$T_{w,\infty}(t) = T_{w,i} + \Delta T_0(1 - e^{-\tilde{\omega}_w t}) \quad (47)$$

and is shown in Fig. 11. At approximately 0.05 s, the exponential term becomes negligible and the response approaches the step input of $T_{w,i} + \Delta T_0$.

(iii) Pulse input. The pulse input approximates flight through thermals. The transformed input is $\Delta T_0 s^{-1}(1 - e^{-\tau s})$ where ΔT_0 is the pulse height and τ is the pulse width. The pulse input is a step of height ΔT_0 at $t = 0$ and a negative step of height (depth) ΔT_0 at $t = \tau$ seconds later. The exponential term is the transform of a unit step function, $u(t - \tau)$. The response is

$$T_{w,\infty}(t) = T_{w,i} + \Delta T_0 \times \{(1 - e^{-\tilde{\omega}_w t}) - u(t - \tau)[1 - e^{-\tilde{\omega}_w (t-\tau)}]\} \quad (48)$$

and is shown in Fig. 12. For large τ, the response will reach ΔT_0 before the switch occurs. For small τ, the temperature will not reach ΔT_0, and thus the 102 probe will not have a complete response. The determining quantity is $\tilde{\omega}_w^{-1}$ and its magnitude is relative to τ.

(iv) Ramp input. The transformed input is Λs^{-2}, where Λ is the ramp slope (K s^{-1}). The response is

$$T_{w,\infty}(t) = T_{w,i} + \Lambda\left[t + \frac{1}{\tilde{\omega}_w}(e^{-\tilde{\omega}_w t} - 1)\right], \quad (49)$$

and is shown in Fig. 13. At long times, the exponential term decays, but the output lags the input with a difference of $\Lambda\tilde{\omega}_w^{-1}$.

(v) Ramp-level input. As in the pulse input case where a positive step was followed τ seconds later by a negative step, the ramp level is a positive ramp with angle Λ followed by a negative ramp with the same slope at a time τ seconds later. The transformed input is $\Lambda s^{-2}(1 - e^{-\tau s})$, where $\tau = \Delta T_0 \Lambda^{-1}$ and ΔT_0 is the step height. The response is

$$T_{w,\infty}(t) = T_{w,i} + \Lambda\left\langle t + \frac{1}{\tilde{\omega}_w}(e^{-\tilde{\omega}_w t} - 1) - u(t - \tau) \times \left\{(t - \tau) + \frac{1}{\tilde{\omega}_w}[e^{-\tilde{\omega}_w (t-\tau)} - 1]\right\}\right\rangle \quad (50)$$

and is shown in Fig. 14. Unlike the ramp input case, here the response approaches the input, when $t \to \infty$.

2) FINITE-LENGTH WIRE

As was done for the infinite length wire model, the five transformed inputs are applied to the two-time-constant transfer function, and the results are inverted to give the transient responses. (The transformed inputs are unchanged from the infinite-length wire case.)

TABLE 2. Two-time-constant model parameters.

Parameters	Regression	Rosemount (1963)	Lenschow (1972)	Spyers-Duran and Baumgardner (1983)	Friehe and Khelif (1993)
a_1	0.875	0.7		0.7	0.65
ω_1^{-1} (ms)	7.36	15	≃20	45	90
a_2	0.125	0.3		0.3	0.35
ω_2^{-1} (ms)	150	1016.4	≃600	170	500

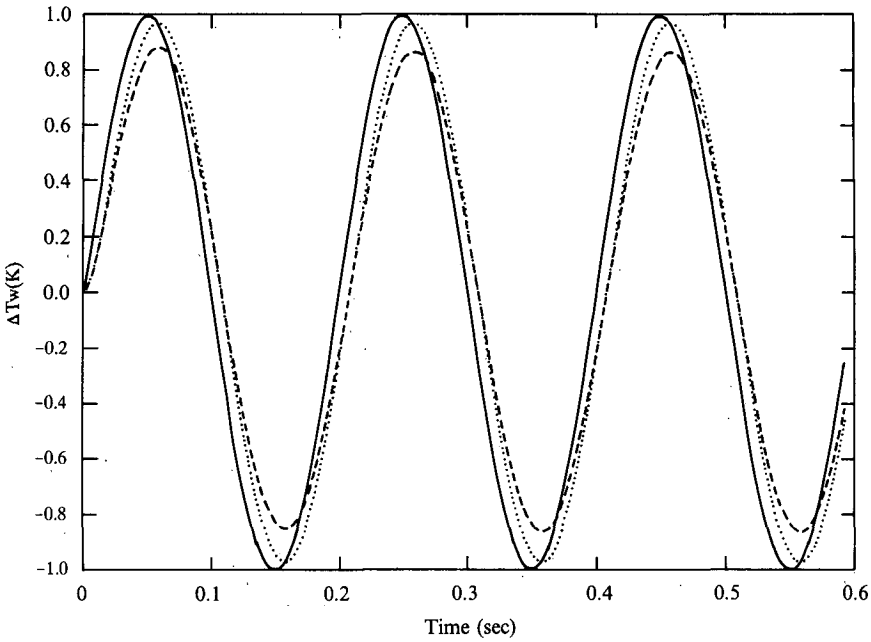

FIG. 10. Time response of the two-time-constant model of the 102 probe and an infinite-length wire to 5-Hz sine wave input having $\Delta T_0 = 1$ K. The solid line is the input, the dotted line is the infinite-length wire response, and the dashed line is the response using the two-time-constant model.

(i) Sinusoidal input. The response is

$$T_{w,tt}(\omega, t) = T_{w,i} + \Delta T_0 M_{w,tt}\Bigg[\sin(\omega t - \phi) + \sin(\phi)\frac{\begin{matrix} a_1\omega_1(\omega_2^2 + \omega^2)e^{-\omega_1 t} \\ + a_2\omega_2(\omega_1^2 + \omega^2)e^{-\omega_2 t} \end{matrix}}{\begin{matrix} a_1\omega_1(\omega_2^2 + \omega^2) \\ + a_2\omega_2(\omega_1^2 + \omega^2) \end{matrix}}\Bigg], \quad (51)$$

where ϕ is $\Phi_{w,tt}(\omega)$ in Eq. (43) and $M_{w,tt}$ is given by Eq. (42). The time response is shown in Fig. 10. The form of Eq. (51) is the same as Eq. (46) except that the amplitude ratio, phase shift, and exponential terms have changed. For the 50-Hz input sine wave, the output is slightly attenuated compared to the infinite-length wire case.

(ii) Step input. The response equation is the same as Eq. (47) with the exponential term modified by the sum of the two time constants. The additional time constant decreases the response, as shown in Fig. 11.

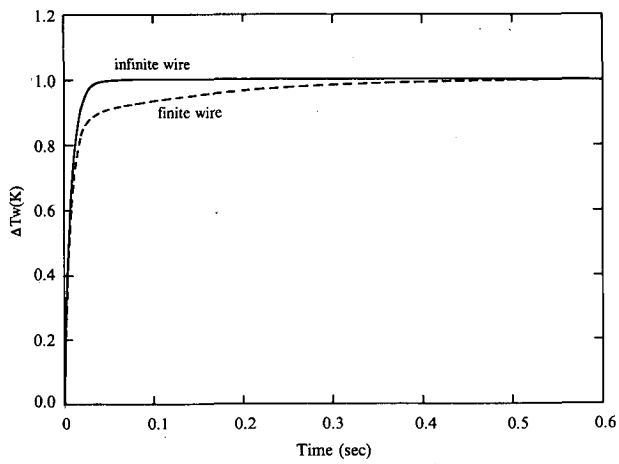

FIG. 11. Time response of the two-time-constant model of the 102 probe and an infinite-length wire to a 1-K step input.

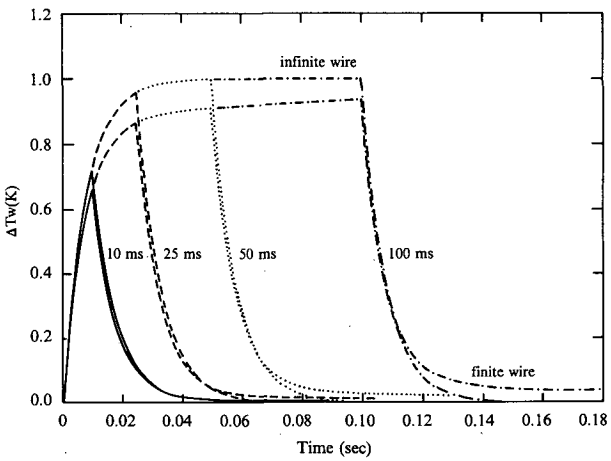

FIG. 12. Time response of the two-time-constant model of the 102 probe and an infinite-length wire to a 1-K-amplitude pulse input of 10-, 25-, 50-, and 100-ms duration.

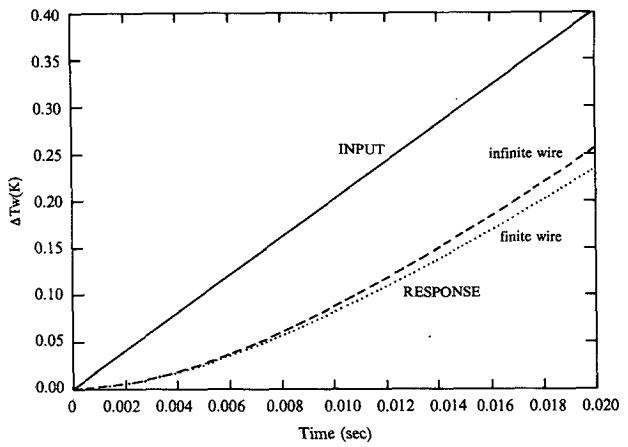

FIG. 13. Time response of the two-time-constant model of the 102 probe and an infinite-length wire to a 20 K s^{-1} ramp input.

(iii) Pulse input. The response is

$$T_{w,tt}(\omega, t) = T_{w,i} + \Delta T_0\{(1 - a_1 e^{-\omega_1 t} - a_2 e^{-\omega_2 t}) - u(t-\tau)[1 - a_1 e^{-\omega_1(t-\tau)} - a_2 e^{-\omega_2(t-\tau)}]\}, \quad (52)$$

and is shown in Fig. 12. Again, the form of the equation is the same as that for the infinite-length wire model except for the added influence of the two time constants.

(iv) Ramp input. The response is

$$T_{w,tt}(t) = T_{w,i} + \Lambda\left[t + \frac{a_1}{\omega_1}(e^{-\omega_1 t} - 1) + \frac{a_2}{\omega_2}(e^{-\omega_2 t} - 1)\right], \quad (53)$$

where Λ is the ramp angle (K s^{-1}). The response is shown in Fig. 13. The difference between input and output at large times is increased over the infinite-length case to $\Lambda(a_1\omega_1^{-1} + a_2\omega_2^{-1})$.

(v) Ramp-level input. The response is

$$T_{w,tt}(t) = T_{w,i} + \Lambda\left[t + \frac{a_1}{\omega_1}(e^{-\omega_1 t} - 1) + \frac{a_2}{\omega_2}(e^{-\omega_2 t} - 1)\right] - u(t-\tau)\Lambda\left\{(t-\tau) + \frac{a_1}{\omega_1} \times [e^{-\omega_1(t-\tau)} - 1] + \frac{a_2}{\omega_2}[e^{-\omega_2(t-\tau)} - 1]\right\}, \quad (54)$$

where, as before, $\tau = \Delta T_0 \Lambda^{-1}$ and ΔT_0 is the input step height. The response has an additional lag caused by the second time constant, as shown in Fig. 14.

4. Discussion

a. Transfer function

The main result of the heat transfer analysis is the derivation of the transfer function of the 102 probe in terms of its geometry, dimensions, physical properties, and heat transfer coefficients, as shown in Fig. 8. The finite-length wire model shows that the effect of conduction to the mica supports occurs for frequencies greater than or equal to 0.1 Hz. It was further shown that the two-time-constant model can be made to agree very well in magnitude and phase with the exact transfer function by the fitting procedure described, leading to the values given in Table 2. However, as shown in Table 2, the present values for ω_1 and ω_2 are smaller than those of Rosemount (1963), Lenschow (1972), Spyers-Duran and Baumgardner (1983), and Friehe and Khelif (1993), while a_1 is larger. The comparison may be compromised as the previous results of Spyers-Duran and Baumgardner and Friehe and Khelif were obtained from in-flight data through thermals or relatively sharp inversions that were assumed to be ideal step functions. A less than ideal step input would result in larger inferred values of ω_2. Also, most in-flight data are not recorded at a high enough rate to adequately measure the fast time constant, ω_1. The values recommended by Rosemount (1963), as well as the in-flight experimental values, also include the effects of the entire housing structure, not just the mica supports.

Comparisons can also be made to the work of Paranthoen et al. (1982) and Lecordier et al. (1984), who modeled laboratory-type probes without the complications of external housings. Their results give a transfer function similar to the present model for various temperature probes with metal supports. For finer diameter wires than modeled in the present study, the amplitude transfer function exhibits a plateau.

When $\omega_1 \gg \omega_2$, as it is in the present model, the second term on the right side of Eq. (39) can be neglected compared to the other terms. Thus,

$$H_{w,tt,a_1=0}(s) \doteq 1 - \frac{a_2 s}{s + \omega_2},$$

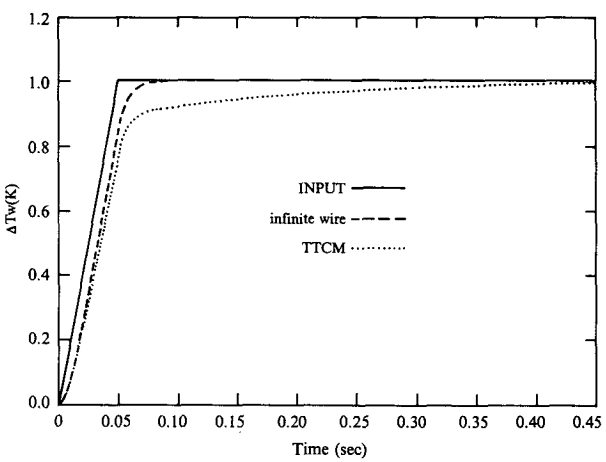

FIG. 14. Time response of the two-time-constant model of the 102 probe and an infinite-length wire to a 20 K s^{-1} ramp for 0.05 s followed by a constant temperature.

which is the same as the transfer function of Paranthoen et al., and

$$a_2 \doteq \frac{1}{\lambda_w L_w}.$$

From the above formula, a_2 is approximately 0.25 as compared to 0.125 from Table 2. The difference can be attributed to the differences in the models, especially in the thermal properties of the supports.

b. *Transient response*

The responses to various input temperature waveforms for both the finite-length and infinite-length (ideal) wires were shown in Figs. 10–14. The degradation of the time response due to the mica supports is clearly evident for the 102 probe, particularly in the case for the pulse and ramp signals, analogous to flying through sharp interfaces of thermals and inversions, respectively. In those situations, the slow response of the mica may considerably mask the true thermal structure of the atmosphere.

5. Conclusions and recommendations

The development of the heat transfer model for the resistance-wire temperature sensor wound on the mica supports in the 102 probe has allowed a quantitative assessment of the time and frequency response of this commonly used aircraft temperature probe. Regression of the complete finite-wire-length model against the simplified two-time-constant model showed that the latter describes the behavior of the probe very well. However, the values of the time constants so obtained do not agree with those from in-flight data or as recommended for the complete 102 probe with external housing. Compared to these, the present model underestimates the degradation in the response. The in situ flight data are probably not very accurate, so a controlled laboratory test to determine the response function of the wire–mica structure and, if possible, the complete 102 probe would be useful.

The transfer function derived here indicates that the 102 probe is adequate for some measurements but not for others. For turbulent heat flux measurements obtained from the covariance of the time series of temperature and vertical velocity, the amplitude response of greater than 0.95 with phase shift of less than 5° for frequencies less than 1 Hz is probably adequate for most atmospheric studies. If we use the largest value of ω_2 [Rosemount (1963)], the transfer function shown in Fig. 15 shows significant attenuation and phase shift below 1 Hz. Ritter et al. (1987) suggest compensating for the transfer function, but since the constants (ω_1, ω_2, a_1, and a_2) involved are not accurately known, the procedure may not produce the correct temperature time series. An alternative is to devise a new probe, as the National Center for Atmospheric Research [see Spyers-Duran and Baumgardner (1983)] and Lawson (1991) have done, or try to improve the 102 design by eliminating the mica support structure as Friehe and Khelif (1993) have done by replacing the platinum wire with a small thermistor bead. However, it is desirable to continue to use strain-free platinum wire for the sensing element, as it is the standard for temperature measurement and maintains a long-term accurate calibration. While the recommendation of Paranthoen et al. (1982) of l/d values of at least 1000 for metal supports cannot probably be met in an aircraft-mounted probe, the present model allows the basic design parameters to be varied to improve the transfer function. For example, reducing the thickness of the mica by a factor of 4 gives the improvement in the transfer function as shown in Fig. 15.

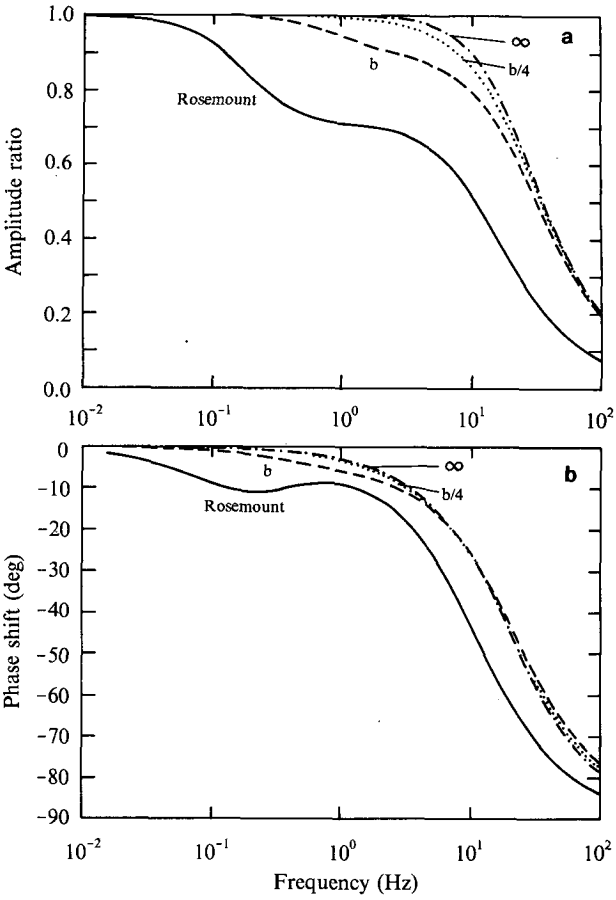

FIG. 15. Comparison of (amplitude) transfer function of Fig. 8 (finite-length wire model) with that recommended by Rosemount (1963) for complete 102 aircraft temperature probe with housing. Also shown is the transfer function for the finite-length wire model with one-fourth thickness mica support.

Acknowledgments. The authors would like to thank Perry L. Fuehrer for his valuable contributions to this work. This work was supported by the National Science Foundation under Grant ATM-9024436 from the Di-

vision of Atmospheric Sciences and Grant N00014-90-1002 from the Marine Meteorology program of the Office of Naval Research. We would like to thank Minh Tsai for his assistance in the preparation of the manuscript and Sue Fisher for the scanning electron microscope photographs.

APPENDIX

Response in Rarefied Flow at Low Reynolds Number

At very low ambient pressures or with wire diameters below about 1 μm, the Nusselt number must be modified to account for rarefied flow where the mean free path of the air molecules is comparable to the wire diameter. Collis and Williams (1956) found that for very low Reynolds numbers in air, $\mathrm{Re} \leq 0.5$, the Nusselt number is

$$\mathrm{Nu}_w = [1.18 + 2\ \mathrm{Kn} - 1.10 \log_{10}(\mathrm{Re}_w)]^{-1},$$

where $\mathrm{Kn} \equiv \lambda_a (2r_w)^{-1}$ is the Knudsen number, λ_a is the mean free path of an air molecule, and Re_w is given by Eq. (4).

It was seen in the transient cases for the infinite-length wire model that $\tilde{\omega}_w$ played an important role. The quantity $\tilde{\omega}_w$ is defined in terms of physical parameters and the wire heat transfer coefficient h_w, which is also a function of the Nusselt number Nu_w. Substituting the above equation for Nu_w into $\tilde{\omega}_w$ and rearranging leads to

$$\frac{1}{\tilde{\omega}_w} = \frac{\rho_w c_w}{4k_a} [2\lambda_a d_w + 1.18 d_w^2 - 1.10 d_w^2 \log_{10}(\mathrm{Re}_w)],$$

where d_w has replaced $2r_w$. This equation is the same as arrived at by LaRue et al. (1975) for the time constant of fine-wire resistance thermometers.

REFERENCES

Chapra, S. C., and R. P. Canale, 1988: *Numerical Methods for Engineers.* McGraw-Hill, 356–357.

Collis, D. C., and M. J. Williams, 1956: Two-dimensional convection from heated wires at low Reynolds numbers. *J. Fluid Mech.*, **6,** 357–384.

Edwards, D. K., V. E. Denny, and A. F. Mills, 1979: *Transfer Processes.* McGraw-Hill, 177–178.

Friehe, C. A., and D. Khelif, 1993: Fast-response aircraft temperature sensors. *J. Atmos. Oceanic Technol.*, **9,** 784–795.

Incropera, F. P., and D. P. Dewitt, 1985: *Introduction to Heat Transfer.* John Wiley and Sons, 177–179.

LaRue, J. C., T. Deaton, and C. H. Gibson, 1975: Measurement of high-frequency turbulent temperature. *Rev. Sci. Instrum.*, **46,** 757–764.

Lawson, R. P., 1991: Design and preliminary tests of a new airborne thermometer. *Seventh Symp. on Meteorological Observations and Instrumentation,* New Orleans, Amer. Meteor. Soc., 366–371.

Lecordier, C., A. Dupont, P. Gajan, and P. Paranthoen, 1984: Correction of temperature fluctuation measurements using cold wires. *Rev. Sci. Instrum.*, **17,** 307–311.

Lenschow, D. H., 1972: The measurement of air velocity and temperature using the NCAR Buffalo aircraft measuring system. NCAR Tech. Notes, NCAR-TN/EDD-74.

Paranthoen, P., C. Petit, and J. C. Lecordier, 1982: The effect of the thermal prong-wire interaction on the response of a cold wire in gaseous flows (air, argon, and helium). *J. Fluid Mech.*, **124,** 457–473.

Ritter, J. A., G. L. Smith, and D. R. Cahoon, 1987: The use of a numerical filter to correct airborne temperature measurements for the effects of sensor lag. *Sixth Symp. on Meteorological Observations and Instrumentation,* New Orleans, Amer. Meteor. Soc., 261–264.

Rosemount, 1963: Total temperature sensors. Rosemount Engineering Company Tech. Bulletin, No. 7637, Eagan, MN, 27 pp.

Shearer, J. L., A. T. Murphy, and H. H. Richardson, 1971: *Introduction to System Dynamics.* Addison-Wesley, 266–283.

Spyers-Duran, P., and D. Baumgardner, 1983: In flight estimation of the time response of airborne temperature sensors. Preprints, *Fifth Symp. on Meteorological Observations and Instrumentation,* Toronto, Amer. Meteor. Soc., 352–357.

Wyngaard, J. C., W. T. Pennell, D. H. Lenschow, and M. A. Lemone, 1978: The temperature–humidity covariance budget in the convective boundary layer. *J. Atmos. Sci.*, **35,** 47–58.